NDT and E International 98 (2018) 45–54

Contents lists available at ScienceDirect

NDT and E International

journal homepage: www.elsevier.com/locate/ndteint

Migration-based automated rebar picking for condition assessment of concrete bridge decks with ground penetrating radar

Kien Dinh [a,*], Nenad Gucunski [b], Trung H. Duong [c]

[a] CONSEN Inc, Montréal, Canada
[b] Department of Civil & Environmental Engineering, Rutgers University, New Jersey, USA
[c] Department of Engineering, Colorado State University-Pueblo, Pueblo, CO, USA

ARTICLE INFO

Keywords:
Ground-penetrating radar
Nondestructive evaluation
Migration
Hyperbolic summation
Automated rebar picking
Image processing

ABSTRACT

Automatic identification and localization of rebar from ground penetrating radar (GPR) data has been a research topic of great interest. This paper presents an automated rebar picking algorithm for GPR data of concrete bridge decks. The algorithm is based on the Limited and Simplified Hyperbolic Summation (LSHS) technique in which the width of migration is limited and a counter is used to check if a hyperbolic signature exist in a sub-region of GPR image. More specifically, after a time-zero correction, each pixel in the raw GPR image with a positive amplitude will be migrated, as it is usually done with the conventional hyperbolic summation (HS) technique. However, for each pixel to be migrated, the width of migration is limited in the horizontal direction and a unit value will be used for migration, instead of the true amplitude values of the pixels. In the obtained image, the pixels containing rebar peaks will normally have the intensity values close to the number of pixels corresponding to the width of migration and, therefore, can be picked. Whereas the method is rather straightforward and simple to develop, its implementation on GPR data of two concrete bridge decks has shown good results. First, the GPR condition maps obtained from the proposed algorithm were in a good agreement with those developed by the manual method of rebar picking. Second, the accuracy of the picking algorithm was 98.09% and 99.21% for the two decks, respectively.

1. Introduction

Ground-penetrating radar (GPR) is a nondestructive evaluation (NDE) technology well suited for concrete bridge deck inspection [1–10]. For each bridge deck, the technology provides a huge amount of data that can be employed to evaluate the deck condition. This large amount of data, however, requires significant processing efforts that are usually time consuming and labor intensive. Therefore, an automation of GPR data analysis will save a considerable amount of time and labor resources for those NDE teams conducting GPR surveys on bridge decks. Moreover, the need of automatic rebar localization is also of increasing importance when the use of robotics assisted bridge deck inspection tools, such as the system described by Gucunski et al. [11], is becoming a reality.

Manual numeric evaluation of GPR data for a bridge deck involves a number of steps. First, GPR profiles (B-scans) need to be pre-processed to make sure that they are correctly geo-referenced. Then, the processing starts with a time-zero correction for each B-scan. This correction aims at finding the true zero time in the B-scans and is mandatory to, later on, correctly extract the rebar depth information (two-way travel times). The next step, after time-zero correction, is rebar picking. This task is usually labor intensive and has always accounted for most of the time an analyst spends to assess the GPR signals from bridge decks. Finally, following the localization of rebar peaks, the reflection amplitudes obtained from these peaks will be used to generate a GPR condition map. In a case where a considerable variation of rebar depth is observed, a depth correction procedure should be performed on the amplitude data before they are used to develop the condition map [3,4,8]. As one can realize, for a bridge deck with thousands of rebar peaks, it takes an extensive amount of time to complete the entire process. Motivated by this problem, the main goal of this study was to develop a system that can automate the rebar-picking task. Accordingly, two research objectives were identified as follows:

(i) Review methods for automatic rebar detection and localization from GPR signals; and

* Corresponding author.
E-mail addresses: kien.dinh@consen.ca (K. Dinh), gucunski@soe.rutgers.edu (N. Gucunski), trung.duong@csupueblo.edu (T.H. Duong).

https://doi.org/10.1016/j.ndteint.2018.04.009
Received 30 October 2017; Received in revised form 2 March 2018; Accepted 15 April 2018
Available online 19 April 2018

(ii) Develop an automated system for picking rebars from bridge deck GPR data.

2. Methods for automatic rebar detection and localization

2.1. Rebar signature in GPR images

This section explains the formation of a rebar signature in GPR B-scans of concrete bridge decks. It is noted herein that a ground-coupled GPR system is used in this research. As can be seen in Fig. 1a, the GPR system comprises two antenna elements, a transmitter (T) and a receiver (R), which are protected in a plastic box, i.e., antenna housing. For each scanning position, the transmitter emits a short pulse of an electromagnetic (EM) wave. The EM wave then propagates through concrete and a part of its energy will be reflected back when it reaches an interface between two media of different dielectric constants. The receiver will record the reflected energy to form an A-scan for each survey location. In concrete decks, common reflection interfaces are air/asphalt and asphalt/concrete (for concrete decks with an asphalt overlay), or air/concrete (for bare concrete decks), concrete/rebar at the top and bottom rebar mats, and finally concrete/air at the deck bottom. Of all the reflectors, concrete/rebar is the most notable interface with a strong amplitude of reflection.

Also illustrated in Fig. 1a is the formation of a GPR B-scan for a bare concrete deck from the records of three scanning positions, which correspond to three A-scans. This B-scan is produced when the GPR antenna passes over a rebar location. It should be noted that, for simplicity, the direct-coupling reflection is not depicted in the diagram. Such a reflection is a mixture of an "air wave", i.e. cross-talk between the transmitter and receiver, and the surface reflection at top of the deck. With respect to the rebar reflection, as can be seen from three scanning positions, it forms a hyperbolic pattern. This occurs as the A-scans are always plotted vertically instead of following the true travel path of the EM wave. It is also worth to note that finding the true travel path of the EM wave reflection in an A-scan is not possible. However, that can be done in B-scans using a so-called "migration" technique. A detailed description and explanation of the technique will be provided later in the research methodology section.

Additional explanations are needed for a more complete comprehension of B-scans from real bridge decks, such as the one depicted in Fig. 1b. Specifically, instead of seeing GPR waveforms, a gray-scale image is shown. This happens because commonly used GPR data processing software automatically converts sampled amplitude values in A-scans into the intensity values of the image pixels. In the GPR images, the horizontal axis depicts the measurement distance, while the vertical axis indicates the depth-related information, for example, two-way travel time. The observed width of a hyperbola in a B-scan will depend on the number of A-scans per unit length and the depth of the corresponding rebar. The higher number of scans per unit length, the wider the hyperbolas will be. Similarly, the deeper a rebar is, the wider the corresponding hyperbola will be.

2.2. Automatic rebar identification

In principle, the assessment of concrete bridge decks from GPR data is based on the evaluation of signal strength at rebar locations [4,6–10]. A strong reflection indicates a sound concrete whereas a low signal amplitude suggests a corrosive environment. Therefore, an automatic condition assessment of concrete bridge decks from GPR data totally depends on the ability to automate the detection and localization of rebars. A summary of previous research ideas to automate the detection and localization of circular objects, in general [12–14], and rebar objects, in particular [15–19], is provided below.

Hyperbolic signatures have been used extensively to detect buried objects in GPR images. Different methods have been proposed to perform this detection. For example, Al-Nuaimy et al. [12] used a neural network classifier that had been trained to divide GPR images into useful and redundant regions. Some further processing and then a Hough Transform was applied to the edges of those useful regions to identify the depth and position of the objects under investigation. In another research, Gamba and Lossani [13] also used a neural network, but to detect hyperbolic pipe signatures, after some preprocessing steps on GPR images had been done. Pasolli et al. [14] proposed another technique that utilized a genetic algorithm to detect linear and hyperbolic patterns in binary images that had been obtained from the two previous steps of preprocessing and thresholding. The hyperbolic patterns were then differentiated from the linear ones by a support vector machine (SVM) classifier.

With regard to rebar detection, Krause et al. [15] came up with an idea of using image segmentation for the detection of hyperbolic signatures. In their research, first, an image segmentation algorithm was used to isolate the arcs in the GPR profiles. From those arcs, hyperbolic shapes would be detected using an arc detector whose principle was based on rating how well an arc matched a hyperbola. In terms of experimental results, the accuracy of the proposed method was reported to be approximately 90% for simple GPR profiles. Nevertheless, that accuracy was substantially reduced when the same algorithm was implemented for more complicated GPR scans.

In 2005, Shaw et al. [16] started using neural networks for the detection of rebars. More specifically, to identify rebars, they first used an image processing technique to detect edge lines in GPR scans. Those identified edge lines were then split into a set of overlapping subsections that were utilized to find hyperbolic patterns using neural networks. The methodology was then verified with a correct detection of two reinforcing bars in a concrete slab. It is, however, obvious that the

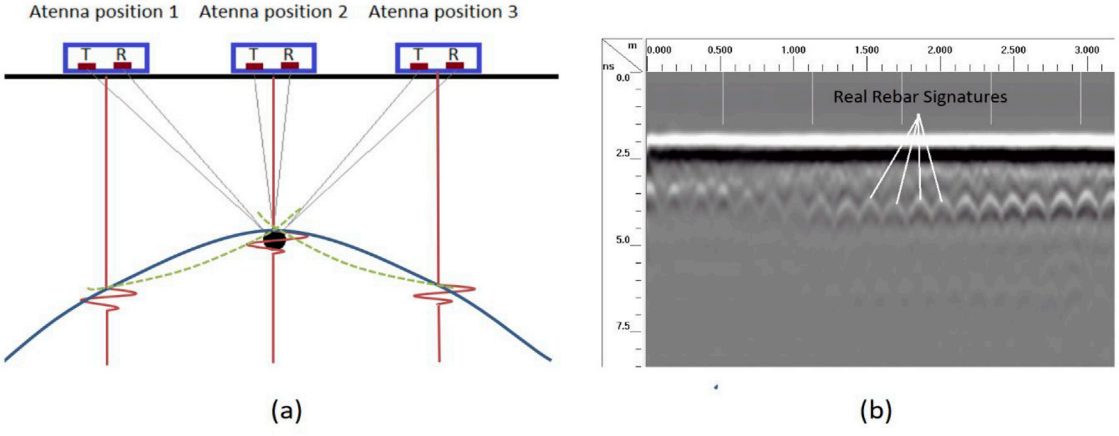

Fig. 1. Formation of hyperbolic rebar signature in (a) schematic and (b) real GPR B-scans.

arrangement of rebars in real concrete decks and in real GPR images is much more complicated than the one illustrated in the case study. Therefore, the application of such a method would be much more difficult.

The use of a template matching and hyperbolic curve fitting to detect reinforcing bars was presented by Wang el al. in Ref. [17]. Specifically, a sum of squared difference (SSD) was used in that research as a similarity metric when a sliding window of GPR images was compared with a hyperbolic rebar template. When the SSD reached a minimum, a reference rebar apex position was selected. Next, with an assumption that the interval between rebars was fixed, a Fast Fourier Transform (FFT) was used to find the hyperbolic apexes of all the remaining rebars. Ultimately, a hyperbolic curve-fitting algorithm was performed to find the parameters of each hyperbola using partial differential equations. As can be realized, such a method has several limitations. First, a rebar template would need to be chosen manually for each individual bridge deck. Second, the assumption of a fixed rebar interval is usually not correct in most cases. In addition, the SSD is not a good similarity metric for the template matching for this kind of a problem. Obviously, the SSD is subjected to the absolute intensity values of the pixels of the two images under comparison.

Kaur et al. [18] employed the support vector machine (SVM) technique to classify a region in GPR images into two categories: containing, and not containing rebar signatures. The input of the SVM classifier was a feature vector extracted from a windowed image region on the investigated B-scan. By comparing the performance of different feature vectors such as the histogram of oriented gradients (HOG), gradient-orientation histogram, maximum gradient orientation, and edge pixels, it was found that the HOG was best suited for the SVM classifier. After finding likely rebar regions using the SVM technique, a hyperbola-fitting algorithm would be used to find rebar peaks in GPR images. The methodology was showcased for two real concrete decks with the correct rebar detection reported as 92.45% and 91.50%, respectively.

Most recently, Dinh et al. [19] proposed a two-step algorithm for an automatic localization and detection of rebars from B-scans of bare concrete bridge decks. In the first step of the algorithm, the hyperbolic summation (HS) migration was used, along with conventional image processing techniques such as normalized cross correlation and thresholding, to locate potential pixels containing rebar peaks. Then, in the second step, a trained convolutional neural network (CNN) was employed to eliminate the false positive detections from the first step. Whereas the algorithm has been proven effective, with an overall accuracy of $99.60 \pm 0.85\%$ for twenty-six concrete bridge decks, it is more computationally expensive than the method developed in this research, as it will be explained later.

3. Research methodology

3.1. Study hypothesis

Rebar picking is the process of identifying and locating the true locations of rebars on GPR scans from the hyperbolic signatures associated with the rebars. As previously explained, the true location of a rebar on GPR scans is considered to be at the apex of the corresponding hyperbola. Therefore, to develop an automated picking algorithm, it is first assumed that a pixel is being considered if it is the apex of a hyperbolic rebar signature. As can be realized, if this is really the case, based on the location of that pixel and GPR signal velocity, it will be possible to calculate the parameters of such a hyperbola, and to find its corresponding location (trace) on each of A-scans adjacent to the pixel. Once this has been done, if only the positive part of the hyperbola is concerned, the pixels on the trace of the hyperbola on each of those A-scans should have positive amplitude values. It is hypothesized that this may be used as a useful condition to verify if the pixel in question is truly an apex of a hyperbolic rebar signature.

3.2. Picking algorithm

To implement and test the hypothesis above, this study developed a simple technique called *L*imited and *S*implified *H*yperbolic *S*ummation, which is abbreviated henceforth as LSHS. While the overall flowchart of the picking algorithm is provided in Fig. 2, details of each of the steps will be described and discussed in the subsequent sections.

3.2.1. Time-zero correction

The time-zero correction is the first step that has to be taken before performing a migration operation on a B-scan. This step is also of importance for an accurate extraction of the two-way travel time and all depth-related information. The zero time corresponds to the first reflection from the ground surface and, conventionally, it is placed at either the negative or the positive maximum peaks of the first wavelet. As this method does not give a very accurate representation of the true time-zero position, the current research employs the zero time suggested by Yelf in Ref. [20]. Specifically, the correct zero time is located at 0.61 ns before

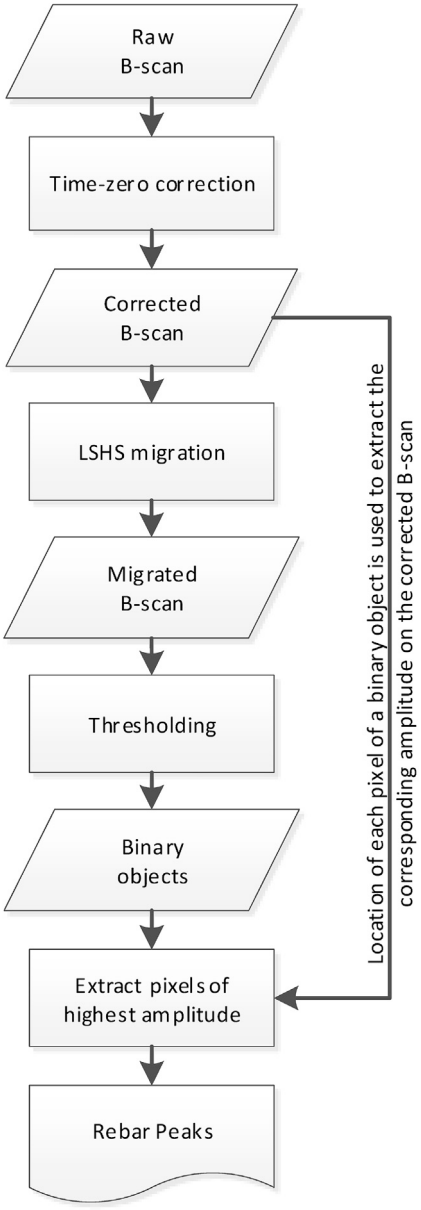

Fig. 2. Picking algorithm.

the positive peak in the first GPR wavelet. Programmatically, this zero time can be found easily for each GPR B-scan.

3.2.2. Limited and Simplified Hyperbolic Summation (LSHS)

This section describes in detail the second step of the picking algorithm where the LSHS migration is performed. For a better comprehension, the hyperbolic summation (HS), the commonly used migration technique, will be explained first. Specifically, the purpose of a migration is to collapse hyperbolic patterns associated with point-like reflecting objects in a B-scan [21]. With respect to the HS algorithm, its principle can be understood through investigating the formation of hyperbolic signature in Fig. 1a. In applying the HS algorithm, each pixel in the original GPR images will be migrated by searching all possible spatial locations of the reflecting object. By doing this, the intensity values of the pixels at a true object location will end up having the sum intensity value of all the pixels on the hyperbolic signature. Therefore, in the migrated GPR profiles, the energy will be focused on those pixels. A comparison between an original B-scan for a concrete bridge deck and the one after migration (with a signal velocity of 0.1 m/ns) is provided in Fig. 3. As can be seen, the B-scan in Fig. 3b provides a much better visualization of the locations of rebars.

Mathematically, the name of HS correctly indicates its working principle. The method considers each pixel in the original GPR image to be the apex of a hypothetical hyperbola. Based on the location of a pixel and an assumed signal velocity, it then determines the shape and location of the corresponding hyperbola in the GPR image. Next, the amplitude values of all the pixels within that shape will be added up to the one of the pixel in question. If the assumption is correct, the amplitude of the pixel will be amplified after migration. If not, its amplitude will become relatively small, compared to those of the pixels containing the apexes of true hyperbolic rebar signatures.

With respect to the signal velocity used for performing the migration, if a velocity lower or higher than the true velocity is selected for the migration, it will result in what is called “under-migration” or “over-migration”. Fig. 4 presents examples of such situations where under-migration (Fig. 4a) and over-migration (Fig. 4b) occur when a B-scan is migrated with a signal velocity of 0.07 m/ns and 0.13 m/ns, respectively. Although the signal velocity may vary among bridge decks and between different regions of the same deck, subjected to the microstructure and moisture content of the concrete cover, based on the experiment on GPR data for many bridge decks, an average signal velocity of 0.1 m/ns has been selected in this research.

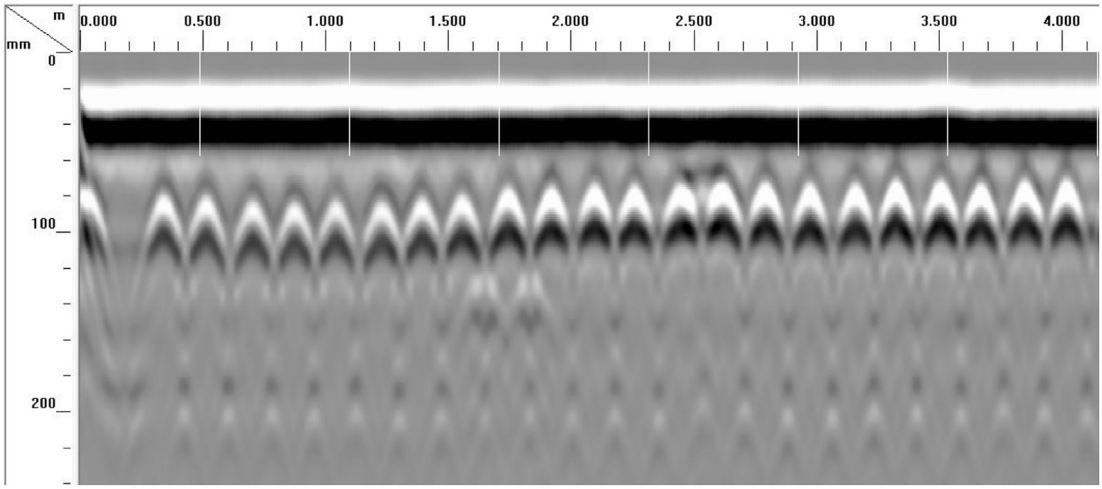

(a)

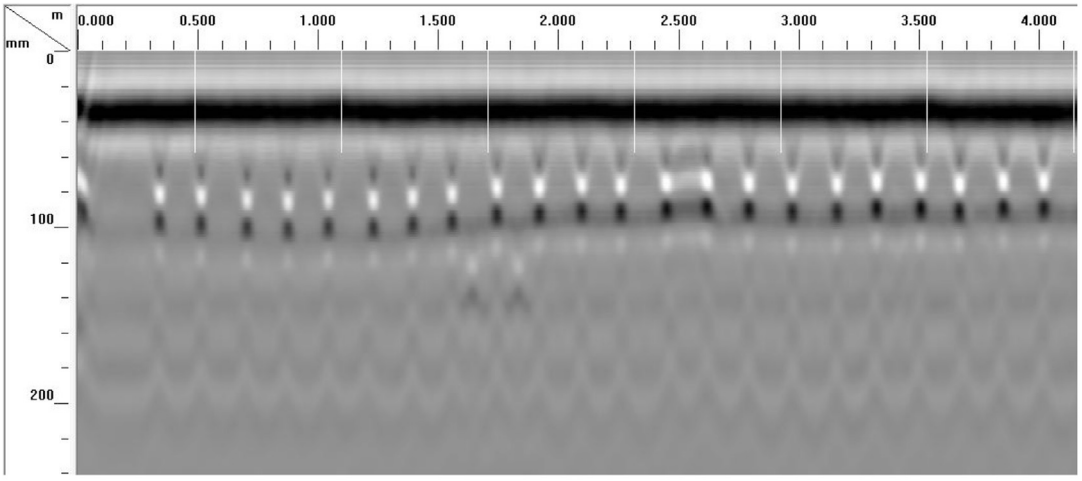

(b)

Fig. 3. B-scans: (a) original and (b) after migration.

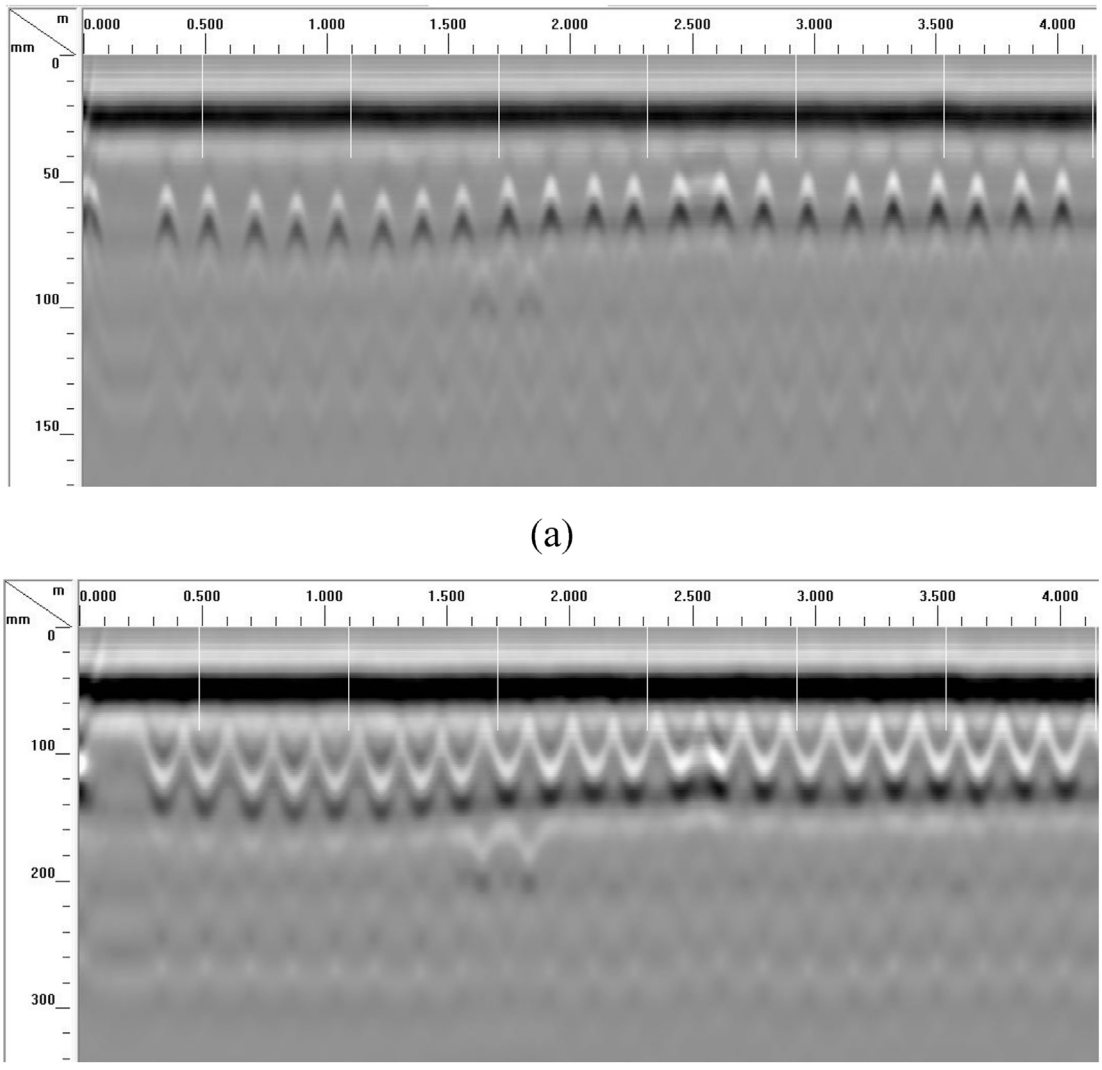

Fig. 4. Migrated B-scans (a) under-migration and (b) over-migration.

As the name implies, the LSHS migration developed in this research is based on the same principle as the HS, but with two major modifications. Fig. 5 illustrates these modifications, where the migration algorithm is performed for the two pixels in green color. As can be seen, the first modification is that the LSHS limits the width (range) of migration to 12 cm, which, as will be explained later, corresponds to the smallest width of a hyperbolic rebar signature. With respect to the second modification, the migration will only be done for the pixels with positive amplitudes. However, instead of using the true amplitudes of the pixels, a unit value will be utilized.

A detailed explanation is needed to justify the width of migration specified above. As illustrated in Fig. 6, due to the effects of a limited antenna beam angle, and the variation of rebar depth, some hyperbolas may appear in the B-scans narrower than the others may. Specifically, among the three test locations depicted in Fig. 6, the reflection from the top rebar will exist only in one A-scan, i.e., the A-scan corresponding to the middle test location. On the other hand, with a greater depth, the bottom rebar will appear in the A-scans of all the depicted test locations. It should be emphasized that, with a high number of scans per unit length commonly used in data collection, in most cases the reflection from a rebar will exist in more than one A-scan, in the form of a hyperbola. However, the number of A-scans in which the reflection from a rebar is present will vary, depending on the depth of that particular rebar. A similar explanation of the beam angle effect can also be found in Ref. [22] for the same 1.6 GHz antenna employed in this study.

For the above reason, it is first necessary to study the size (width) of hyperbolic rebar signatures commonly found in GPR B-scans of concrete bridge decks. In other words, an answer to the following question is needed: what is the smallest width of a hyperbolic rebar signature in the horizontal direction? Mathematically, this information can be obtained, if the exact antenna beam angle is known. However, as the authors do not have such a detailed information, an empirical approach was selected for this study. Specifically, an observation from a review of a large number of GPR data for bridge decks has allowed this value to be identified as being approximately 12 cm. It means, to implement the research idea, the picking algorithm should only find the trace of the hypothetical hyperbola in the A-scans within a horizontal distance of 6 cm from the pixel under investigation, i.e., the apex of the hypothetical hyperbola.

With respect to the second modification of using a unit amplitude value in the migration, its aim was to check whether all the pixels on the traces of hypothetical hyperbolas have positive amplitudes, or not. In other words, the LSHS algorithm allows the creation of a simple counting

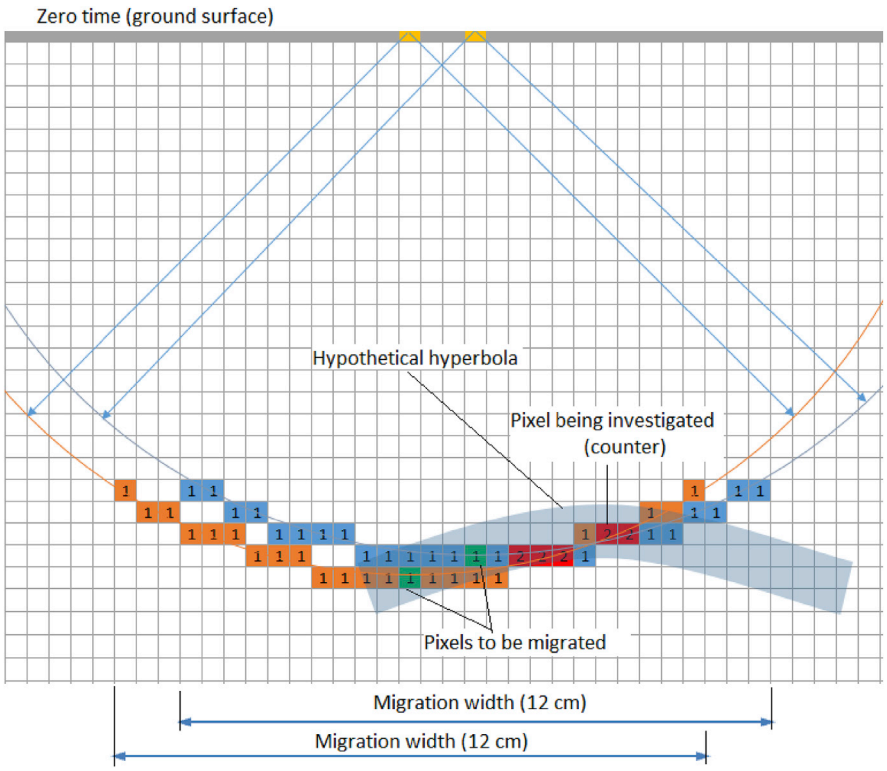

Fig. 5. Understanding the limited and simplified hyperbolic summation (LSHS).

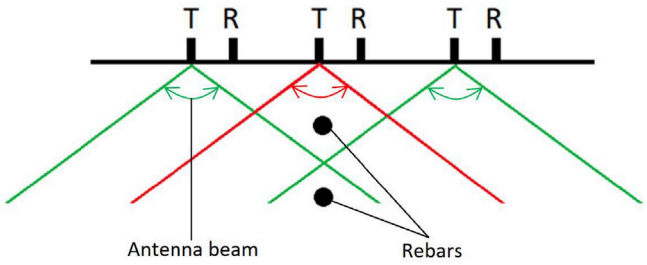

Fig. 6. Effects of antenna beam and rebar depth to the width of rebar signatures.

system that can be used to verify if a hypothetical hyperbola is truly a rebar signature. Specifically, supposing that on each of the traces of the hypothetical hyperbola within a horizontal distance of 6 cm from its hypothetical apex, a pixel is taken and its amplitude is examined. If the amplitude is positive, a unit amplitude value will be assigned to that pixel and be added to a counter, which is located at the apex of the hyperbola. If not, the counter will remain the same. After this procedure has been done for all A-scans within the scope of the algorithm, for a true hyperbolic rebar signature, the counter should have the value being equal to the number of A-scans. This idea is illustrated in Fig. 7 where the red pixel in Fig. 7a is likely a rebar peak whereas the green pixel in Fig. 7b is not likely a rebar peak.

3.2.3. *Thresholding*

As explained above, the purpose of using a unit amplitude value in the operation of LSHS is to count the number of A-scans that have positive amplitudes (indicating reflection) within the shape of the hypothetical hyperbola. If this number is equal to the maximum number of A-scans within the width of LSHS migration, it is likely that the pixel in question is the apex of a hyperbolic rebar signature. However, the use of such an extreme threshold (no tolerance) may result in a failure of the algorithm in picking rebars within certain areas in a B-scan. The first reason is that

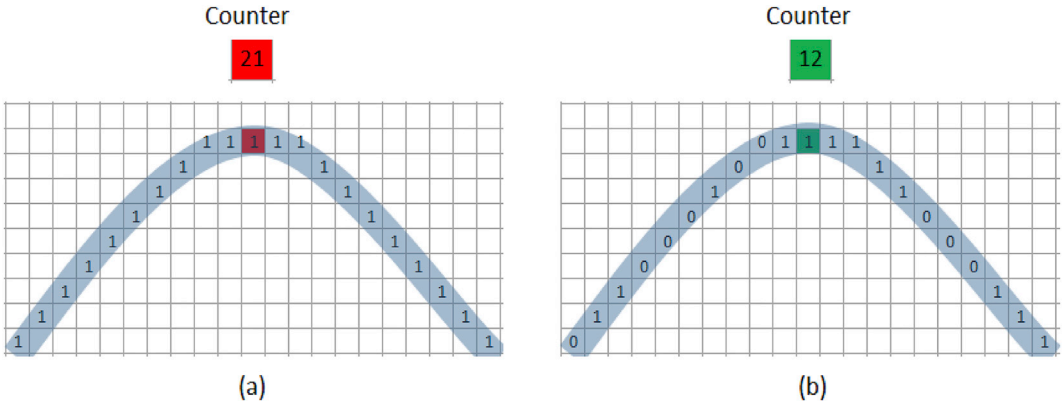

Fig. 7. Hypothetical hyperbolas: (a) likely and (b) unlikely rebar peaks.

some hyperbolic shapes may be distorted due to a concrete damage, a bump on the deck surface during the data collection, or due to some other reasons. The second reason is that some of the signals on a hyperbola may be too weak (zero amplitude), because of a corrosive environment. Thus, those are not migrated to the apex of the hyperbola. The third reason is that, for some decks, the true signal velocity may vary between deck areas. Consequently, the under- or over-migration may occur in some of those areas. Finally, the algorithm may fail simply as a result of digital sampling. For example, as can be seen in Fig. 5, there are several instances where the LSHS algorithm needs to decide on which of the two pixels in the same column the migration should be performed. For all these reasons, if an extreme threshold is used, one defective pixel on the trace of a correct rebar signature might lead to a failure of the algorithm in picking that rebar. Therefore, it may be more reasonable to select a smaller threshold for the picking algorithm. However, that may lead to another issue, the false positive detection, where some reflections from other objects may be misclassified as rebar peaks.

3.2.4. Extract rebar peaks

As will be seen in the experiment section, the output of thresholding a migrated B-scan will be binary objects containing pixels of potential rebar peaks. The reason being to obtain high-resolution images, the sampling frequency is normally set high enough, so that each reflection wavelet will contain many more than one digitized sample. Correspondingly, the algorithm will need to select from those objects the pixels that best represent the apex of each hyperbola. While the selection of the rebar peaks in those cases might be done by simply finding the centroid of the candidate pixels, or the pixel with the highest amplitude, the latter has been used in this study.

3.3. Experiments

A program has been written in MATLAB to implement the proposed algorithm. In the program, the user is allowed to change both the width of migration and the picking threshold. However, as the width of migration has been selected previously to be 12 cm, in the first experiment shown in Fig. 8, only the threshold will be varied to observe the corresponding change in the picking performance of the proposed algorithm. Specifically, the picking performance for a B-scan, when the picking threshold is set to correspond to 12, 11 and 10 cm, is depicted in Fig. 8a, b, and c, respectively. As can be seen, when the threshold is set to 12 cm, the algorithm fails to detect some of the rebars. When the threshold is reduced to 11 cm, all the rebars are detected. However, when the threshold is set to 10 cm, a number of false positive peaks appear. As the performance is the best when the threshold is set to 11 cm, that threshold is used in the second experiment, which follows.

The purpose of the second experiment was to see, if there is any effect of rebar spacing on the performance of the picking algorithm. Specifically, whereas the average spacing distance between rebars in the first experiment in Fig. 8 is 16 cm, the average value for the second experiment is only 9 cm. With the same threshold, which was selected to be equivalent to the number of A-scans in a horizontal distance of 11 cm, the picking performance is presented in Fig. 9. The result indicates that all rebar peaks in the original GPR image in Fig. 9a have been successfully localized by the developed algorithm in Fig. 9e. It suggests that the distance between rebars is not a factor that affects the picking algorithm. It

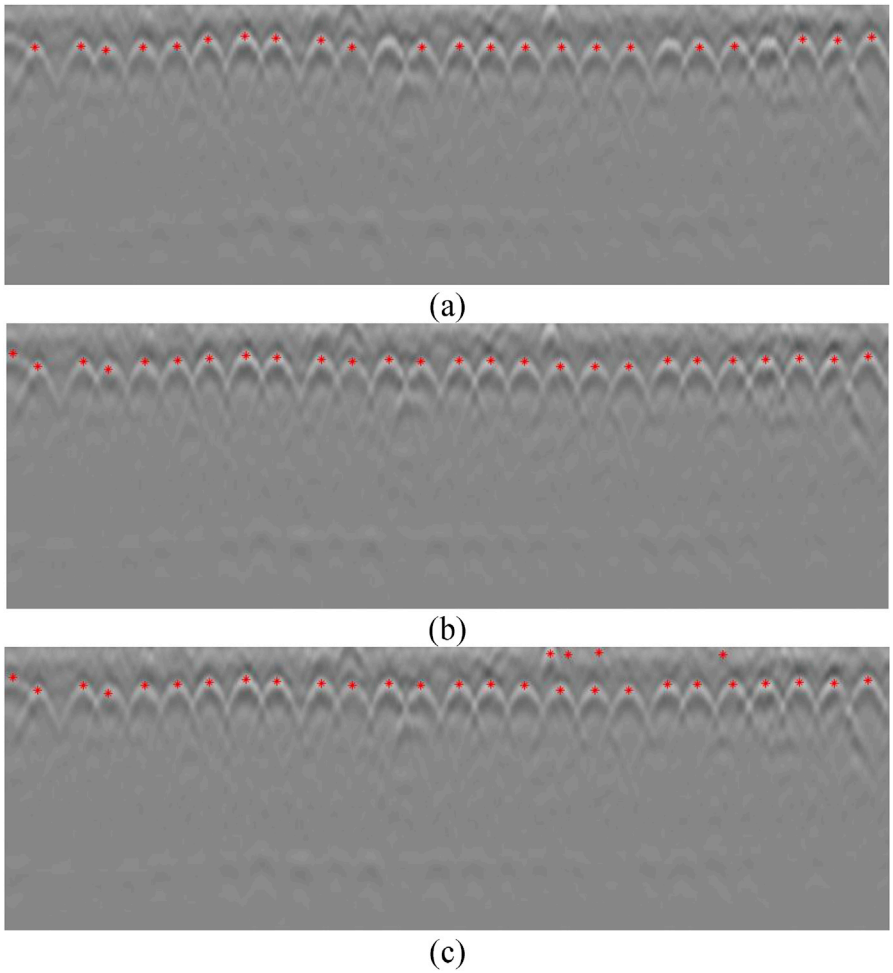

Fig. 8. Performance of rebar picking algorithm when the threshold is set to (a) 12 cm, (b) 11 cm and (c) 10 cm.

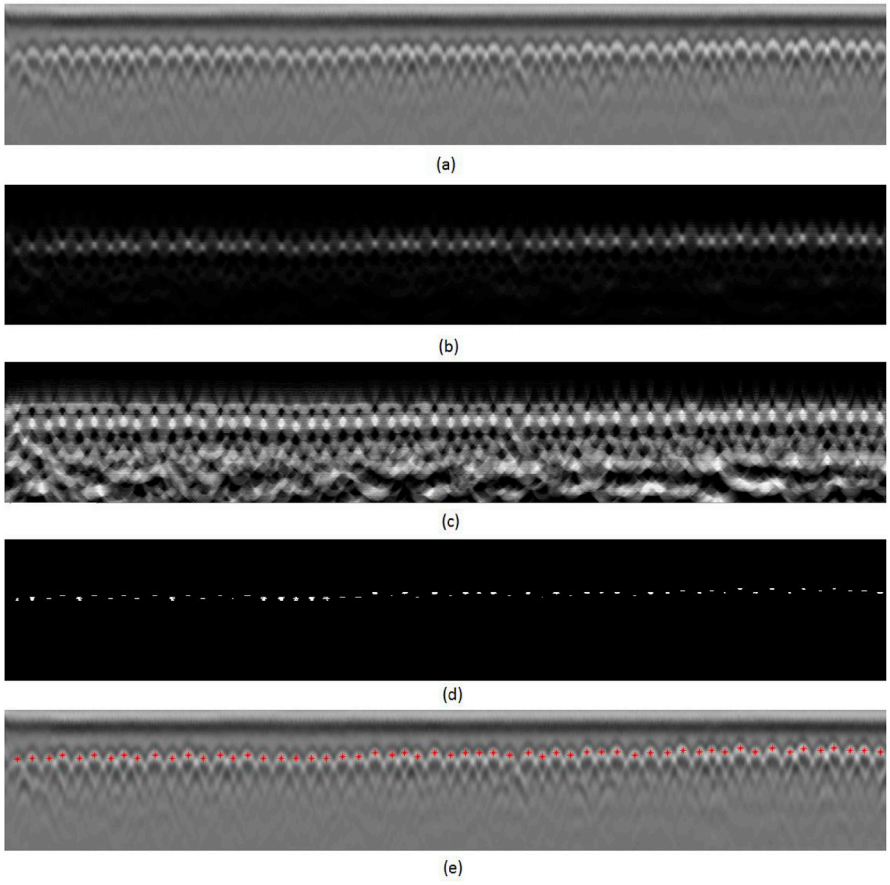

Fig. 9. GPR scans (a) original, (b) after HS migration, (c) after LSHS migration, (d) after thresholding, and (e) with rebar picking.

is noted that, for a comparison, the migrated B-scan using the conventional HS is also included in Fig. 9b. As can be seen, whereas the migrated GPR scan using the conventional technique provides a much better contrast than the one using the proposed LSHS (Fig. 9c), it contains a less useful information, in terms of providing the rebar picking criteria. Specifically, in the migrated B-scan using HS, the intensity (amplitude) values of the pixels containing rebar peaks may vary between different bars. Therefore, the rebars cannot be picked based on the amplitude. That was the reason why Dinh et al. [19] had to use a CNN in the second step of their algorithm. On the other hand, by limiting the width of migration and using a counting system (counter), the proposed LSHS algorithm allows the rebars to be picked by simply using the amplitude criterion. Therefore, the algorithm developed in this research is less computationally demanding than the one described in Ref. [19]. Specifically, for the B-scan in the second experiment, which is 64 m long, while the execution time of the algorithm proposed in Ref. [19] was 28 s, the time needed for the proposed algorithm was only 10 s. The computer, which was used for the comparison, has 16.0 GB of installed memory (RAM) and a 64-bit operating system. The speed of the central processing unit (CPU), as indicated by the system, is 3.50 GHz.

4. Case study implementation

In this section, GPR condition maps will be developed for two real concrete bridge decks using both manual and automated rebar picking. For each deck, the two maps will be compared to examine the performance of the automated rebar-picking algorithm. With respect to the depth correction, both methods will use the same technique described in Ref. [3]. In addition, for each deck, the accuracy of the automatic rebar-picking algorithm will also be investigated by studying the instances of false positive and false negative rebar detection. To clarify, a false positive detection is the case when the algorithm erroneously picks a pixel that is not a rebar peak, while false negative detection is the case when a true rebar peak is overlooked by the automated algorithm. It is noted further that, comparing the number of detected rebar peaks with the one extracted from the design documents was not the objective of this study. As one can realize, the as-built rebar configuration may be, in some cases, somewhat different from the design one. That explains why one of the applications of GPR has been to verify the quality of construction (quality assurance/quality control) [1]. Finally, it is worthy to emphasize that, in the case studies, only the top rebars will be of concern.

4.1. Elkton Bridge, Maryland

The bridge in Elkton, Maryland was constructed in 1973. It is located on State Route 273 and crosses over the Little Elk Creek. The bridge is 27 m long and 14 m wide, which has a bare concrete deck on seven steel girders, and two abutments and a center pier. The bridge is skewed with an angle of $14^0 53'$. The deck, which is 20 cm thick, was tested in July 2013 using a 1.5 GHz ground-coupled GPR antenna manufactured by GSSI. The scan lines were set up parallel to the traffic with a 2-foot spacing distance. The number of scans per unit length was set up to 60 scans/foot. The GPR condition maps developed using the two rebar-picking methods are provided in Fig. 10. As can be seen, the two maps are in good agreement, with a minimum discrepancy. With regard to the performance of the automated rebar picking algorithm, of 2772 rebar peaks in the original GPR profiles, it was able to pick correctly in 2733 and miss in 39 instances. There were 14 instances where a pixel was misclassified as a rebar peak. Accordingly, the accuracy of the algorithm was calculated to be 98.09%.

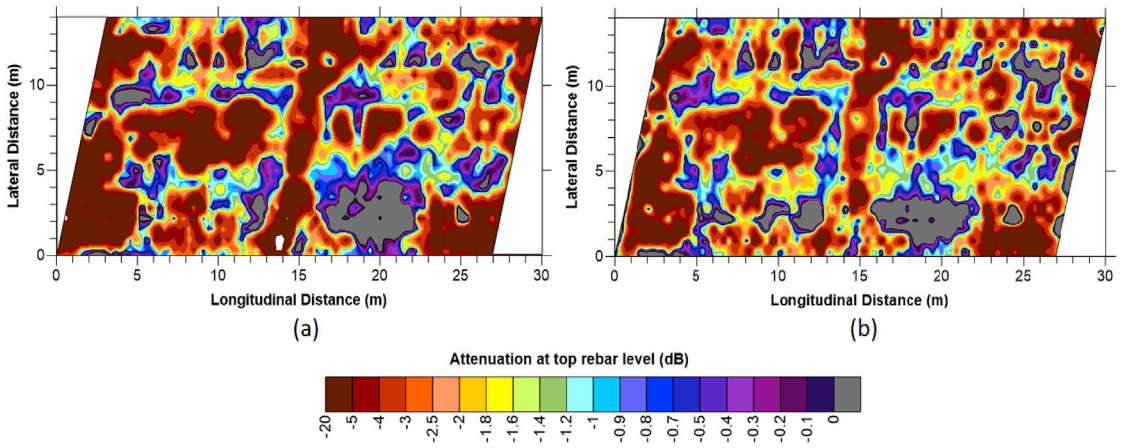

Fig. 10. GPR maps for the Elkton Bridge deck developed with (a) manual, and (b) automated rebar picking.

4.2. *Pequea Bridge, Pennsylvania*

The Pequea Bridge in Conestoga, Pennsylvania, was built in 1970. It is of the same structure type as the Elkton Bridge, i.e., a bare concrete deck on steel girders. The deck of the bridge, which is 47 m long and 13 m wide, was tested in August 2013 using a 1.5 GHz ground-coupled GPR antenna. The survey grid was set up in the same way as on the Elkton Bridge. The GPR condition maps developed with manual and automated rebar picking are provided in Fig. 11. As can be seen, except for some small areas at the bottom of the two maps, they look almost identical. In terms of the accuracy of the automated method, whereas the visual examination indicates a total number of 6867 rebar peaks, 6834 of them were picked correctly. The number of false positive instances was 21. It means that the accuracy of the automated method for the Pequea Bridge deck was 99.21%.

5. Conclusions

Picking rebars from GPR data of concrete bridge decks is time consuming and labor intensive. This paper, therefore, presents a simple algorithm for the automation of that task. As has been seen, the algorithm is based on the idea of the conventional hyperbolic summation technique where it is simplified to provide a suitable condition for the localization of rebar peaks. By limiting the width of migration and using a unit amplitude value for migration, the algorithm has basically created a counting system to verify the continuity of a hyperbolic signature. If this continuity is confirmed, there is likely a rebar peak at the pixel under investigation. As a proof of concept, the proposed algorithm has been implemented for two real concrete bridge decks. In both cases, the condition maps provided by the picking algorithm almost resembled those obtained from the manual rebar picking method. In addition, the accuracy of the proposed picking algorithm was 98.09% and 99.21%, respectively, for the two decks.

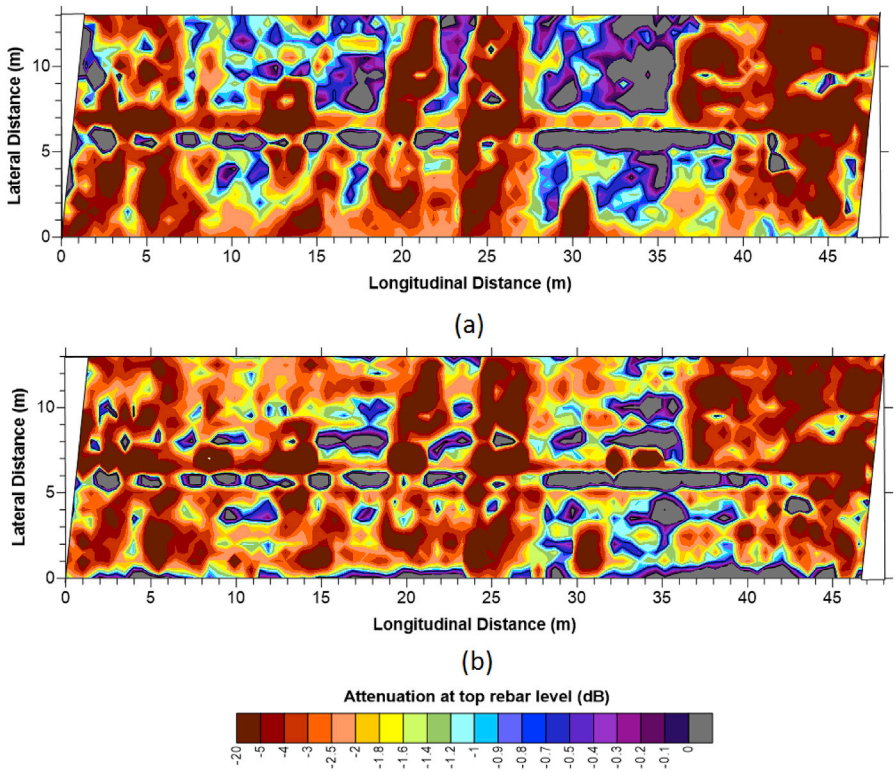

Fig. 11. GPR maps for the Pequea Bridge deck developed with (a) manual, and (b) automated rebar picking.

Acknowledgements

The authors of this study are grateful to the Federal Highway Administration for their support for GPR surveys through the Long-Term Bridge Performance (LTBP) Program.

References

[1] Gucunski N, Imani A, Romero F, Nazarian S, Yuan D, Wiggenhauser H, Shokouhi P, Taffe A, Kutrubes D. Nondestructive testing to identify concrete bridge deck deterioration. Transport Res. Board 2013. https://doi.org/10.17226/22771. Washington D.C,.

[2] Gucunski N, Pailes B, Kim J, Azari H, Dinh K. Capture and quantification of deterioration progression in concrete bridge decks through periodical NDE surveys. J Infrastruct Syst 2016 Jun 17;23(1). https://doi.org/10.1061/(ASCE)IS.1943-555X.0000321. B4016005.

[3] Barnes CL, Trottier JF, Forgeron D. Improved concrete bridge deck evaluation using GPR by accounting for signal depth–amplitude effects. NDT E Int 2008 Sep 30; 41(6). https://doi.org/10.1016/j.ndteint.2008.03.005. 427–33.

[4] Romero FA, Barnes CL, Azari H, Nazarian S, Rascoe CD. Validation of benefits of automated depth correction method: improving accuracy of ground-penetrating radar deck deterioration maps. Transportation research record. J Transp Res Board 2015;1(2522):100–9. https://doi.org/10.3141/2522-10.

[5] Tarussov A, Vandry M, De La Haza A. Condition assessment of concrete structures using a new analysis method: ground-penetrating radar computer-assisted visual interpretation Construct Build Mater, vol. 38; 2013. p. 1246–54. https://doi.org/10.1016/j.conbuildmat.2012.05.026.

[6] Martino N, Birken R, Maser K, Wang M. Developing a deterioration threshold model for the assessment of concrete bridge decks using ground penetrating radar. In: Transportation research board 93rd annual meeting; 2014. p. 14–3861.

[7] Dinh K, Zayed T, Moufti S, Shami A, Jabri A, Abouhamad M, Dawood T. Clustering-based threshold model for condition assessment of concrete bridge decks with ground-penetrating radar. Transport Res Rec J. Transport Res. Board 2015 Aug 1; 2522:81–9. https://doi.org/10.3141/2522-08.

[8] Dinh K, Gucunski N, Kim J, Duong TH. Understanding depth-amplitude effects in assessment of GPR data from concrete bridge decks. NDT E Int 2016 Oct 31;83: 48–58. https://doi.org/10.1016/j.ndteint.2016.06.004.

[9] Dinh K, Zayed T, Romero F, Tarussov A. Method for analyzing time-series GPR data of concrete bridge decks. J Bridge Eng 2014;20(6). https://doi.org/10.1061/(ASCE)BE.1943-5592.0000679. 04014086.

[10] Dinh K, Gucunski N, Kim J, Duong TH. Method for attenuation assessment of GPR data from concrete bridge decks. NDT E Int 2017 Dec 1;92:50–8. https://doi.org/10.1016/j.ndteint.2017.07.016.

[11] Gucunski N, Basily B, Kim J, Jin GY, Duong T, Dinh K, Kee SH, Maher A. RABIT: implementation, performance validation and integration with other robotic platforms for improved management of bridge decks. Int. J. Intell. Robot. Appl. 2017 Jul 17;1(3):271–86. https://doi.org/10.1007/s41315-017-0027-5.

[12] Al-Nuaimy W, Huang Y, Nakhkash M, Fang MTC, Nguyen VT, Eriksen A. Automatic detection of buried utilities and solid objects with GPR using neural networks and pattern recognition. J. Appl. Geophys. 2000;43(2):157–65. https://doi.org/10.1016/S0926-9851(99)00055-5.

[13] Gamba P, Lossani S. Neural detection of pipe signatures in ground penetrating radar images. IEEE Trans Geosci Rem Sens 2000;38(2):790–7. https://doi.org/10.1109/36.842008.

[14] Pasolli E, Melgani F, Donelli M. Automatic analysis of GPR images: a pattern-recognition approach. IEEE Trans Geosci Rem Sens 2009;47(7):2206–17. https://doi.org/10.1109/TGRS.2009.2012701.

[15] Krause, V., Abdel-Qader, I., Abudayyeh, O. and Yehia, S. An image segmentation algorithm for the detection of rebar in bridge decks from GPR scans. In Electro/information technology, 2007 IEEE international conference on (pp. 114–119). IEEE. DOI: 10.1109/EIT.2007.4374476

[16] Shaw MR, Millard SG, Molyneaux TCK, Taylor MJ, Bungey JH. Location of steel reinforcement in concrete using ground penetrating radar and neural networks. NDT E Int 2005;38(3):203–12. https://doi.org/10.1016/j.ndteint.2004.06.011.

[17] Wang ZW, Zhou M, Slabaugh GG, Zhai J, Fang T. Automatic detection of bridge deck condition from ground penetrating radar images. IEEE Trans Autom Sci Eng 2011;8(3):633–40. https://doi.org/10.1109/TASE.2010.2092428.

[18] Kaur P, Dana KJ, Romero FA, Gucunski N. Automated GPR rebar analysis for robotic bridge deck evaluation. IEEE Trans. Cybern. 2016;46(10):2265–76. https://doi.org/10.1109/TCYB.2015.2474747.

[19] Dinh K, Gucunski N, Duong TH. An algorithm for automatic localization and detection of rebars from GPR data of concrete bridge decks. Autom ConStruct 2018 Feb;89:292–8. https://doi.org/10.1016/j.autcon.2018.02.017.

[20] Yelf R. Where is true time zero?. In: Ground. Penetrating radar, 2004. Gpr 2004. Proceedings of the tenth international conference on, vol. 1. IEEE; 2004. p. 279–82. https://doi.org/10.1109/ICGPR.2004.179979.

[21] Daniels DJ. Ground penetrating radar. John Wiley & Sons, Inc; 2005. https://doi.org/10.1002/0471654507.eme152.

[22] Geophysical Survey Systems, Inc. (GSSI). Concrete handbook. 2017. Retrieved from, https://www.geophysical.com/wp-content/uploads/2017/10/GSSI-Concrete-Handbook.pdf. [Accessed 26 February 2018].